Accepted Manuscript

Hydrogel-coated feed spacers in two-phase flow cleaning in spiral wound membrane elements: A novel platform for eco-friendly biofouling mitigation

Yusuf Wibisono, Wetra Yandi, Mohsen Golabi, Roni Nugraha, Emile R. Cornelissen, Antoine J.B. Kemperman, Thomas Ederth, Kitty Nijmeijer

Please cite this article as: Wibisono, Y., Yandi, W., Golabi, M., Nugraha, R., Cornelissen, E.R., Kemperman, A.J.B., Ederth, T., Nijmeijer, K., Hydrogel-coated feed spacers in two-phase flow cleaning in spiral wound membrane elements: A novel platform for eco-friendly biofouling mitigation, *Water Research* (2015), doi: 10.1016/j.watres.2014.12.030.

Graphical abstract

Legend:
- Feed spacer
- Hydrogel
- Bacteria/EPS
- Hydration shell

Hydrogel-coated feed spacers in two-phase flow cleaning in spiral wound membrane elements: a novel platform for eco-friendly biofouling mitigation

Yusuf Wibisono[1,4#], Wetra Yandi[2#], Mohsen Golabi[3], Roni Nugraha[2], Emile R. Cornelissen[5], Antoine J.B. Kemperman[1*], Thomas Ederth[2], Kitty Nijmeijer[1]

[1] University of Twente, Membrane Science and Technology, MESA+ Institute of Nanotechnology, Faculty of Science and Technology, P.O. Box 217, 7500 AE, Enschede, The Netherlands

[2] Linköping University, Division of Molecular Physics, Department of Physics, Chemistry and Biology (IFM), SE-581 83 Linköping, Sweden

[3] Linköping University, Division of Biosensors and Bioelectronics, Department of Physics, Chemistry and Biology (IFM), SE-581 83 Linköping, Sweden

[4] Wetsus, Centre of Excellence for Sustainable Water Technology, P.O. Box 1113, 8900 CC, Leeuwarden, The Netherlands

[5] KWR Watercycle Research Institute, P.O. Box 1072, 3430 BB, Nieuwegein, The Netherlands

#Both authors contributed equally to this work.

*Corresponding author. Tel.: +31-53-4892956; Fax.: +31-53-4894611

Email address: a.j.b.kemperman@utwente.nl (A.J.B. Kemperman)

25 **Keywords:**

26 Hydrogel, charge, biofouling, two-phase flow, feed spacer, spiral-wound membrane

27

28

29 **Abstract**

30 Biofouling is still a major challenge in the application of nanofiltration and reverse osmosis

31 membranes. Here we present a platform approach for environmentally friendly biofouling

32 control using a combination of a hydrogel-coated feed spacer and two-phase flow cleaning.

33 Neutral (polyHEMA-co-PEG$_{10}$MA), cationic (polyDMAEMA) and anionic (polySPMA)

34 hydrogels have been successfully grafted onto polypropylene (PP) feed spacers via plasma-

35 mediated UV-polymerization. These coatings maintained their chemical stability after 7 days

36 incubation in neutral (pH 7), acidic (pH 5) and basic (pH 9) environments. Anti-biofouling

37 properties of these coatings were evaluated by *E. coli* attachment assay and nanofiltration

38 experiments at a TMP of 600 kPag using tap water with additional nutrients as feed and by

39 using optical coherence tomography. Especially the anionic polySPMA-coated PP feed spacer

40 shows reduced attachment of *E. coli* and biofouling in the spacer-filled narrow channels

41 resulting in delayed biofilm growth. Employing this highly hydrophilic coating during

42 removal of biofouling by two-phase flow cleaning also showed enhanced cleaning efficiency,

43 feed channel pressure drop and flux recoveries. The strong hydrophilic nature and the

44 presence of negative charge on polySPMA are most probably responsible for the improved

45 antifouling behavior. A combination of polySPMA-coated PP feed spacers and two-phase

46 flow cleaning therefore is promising and an environmentally friendly approach to control

47 biofouling in NF/RO systems employing spiral-wound membrane modules.

48

49

1. Introduction

High pressure membrane processes, *i.e.* nanofiltration (NF) and reverse osmosis (RO) are the most commonly applied membrane processes for the removal of contaminants and pathogens from drinking water supplies (Greenlee et al. 2009, Hilal et al. 2004). However, despite their widespread application worldwide, biofouling remains a major obstacle since it lowers the performance of NF/RO plants (Matin et al. 2011).

Commonly practiced biofouling control by using chemical agents (alkalines, detergents, enzymes, chelating agents, acids, biocides) were found ineffective in removing biofouling completely from NF/RO spiral wound membrane channels (Creber et al. 2010, Hijnen et al. 2012). Besides promoting membrane damages and being harmful to the environment , the use of biocides may promote the resistance of microorganisms towards these biocides and worsen the biofouling problems (Applegate et al. 1989). Re-growth of biofouling was observed after chemical cleaning, due to the presence of dead bacteria, which served as nutrients for subsequent growth. Physical removal of remaining biomass is therefore essential to optimize biofouling control (Bereschenko et al. 2011). The presence of spacers in the membrane modules has a significant contribution to the occurrence of biofouling and especially the feed spacer is a source for biomass growth inducing befouling. Biofouling removal from membrane feed channels using two-phase flow was found effective and can be used as an environment and membrane friendly cleaning method (Wibisono et al. 2014, Wibisono et al. 2015).

In our previous work, we investigated the role of feed spacer geometry, feed pressure, gas/liquid ratio, cleaning duration, and liquid velocity on biofouling removal in spiral wound membrane elements (Wibisono et al. 2015). However, in order to reduce the occurrence of biofouling, prevention at the source is the preferred option. In this work we therefore investigate the influence of charge of the employed spacers using hydrogel coated

3

75   polypropylene (PP) feed spacers, and its effect on prevention of early attachment of

76   biofouling. Although the effect of charge on the anti-biofouling properties has been

77   investigated before, the effect of charge of a polymer coated feed spacer filament has

78   however, not been investigated systematically so far. Three hydrogels with different charge

79   (neutral: polyHEMA-co-PEG$_{10}$MA; cationic: polyDMAEMA and anionic: polySPMA) were

80   selected and coated onto a polypropylene (PP) feed spacer. Considering previous work on

81   charge-balanced materials, such as zwitterionic or pseudo-zwitterionic coatings, these would

82   also be interesting candidates for comparison in a test with charged surfaces, but in view of

83   the excellent performance of polyHEMA-co-PEG$_{10}$MA coatings in marine antifouling

84   applications [Ekblad et al.. 2008], we selected this particular chemistry as the neutral material.

85   We are interested in seeing how charged coatings on the spacers affect the early attachment of

86   biofouling, and how these coatings influence the membrane filtration performance in general.

87   We expect that charge interactions between coating materials in the spacers are highly

88   relevant to study, since fouling microorganisms are normally charged, which also holds true

89   for -macromolecules secreted by the organisms (e.g. polysaccharides, proteins etc.) in the

90   early attachment of biofouling, and this will also affect the performance of membrane

91   filtration NF/RO system. Thus, we systematically investigate the anti-biofouling effect of the

92   feed spacer charge using bacteria attachment tests and biofouling evaluation in nanofiltration

93   experiments. We aim at providing a novel eco-friendly method to control biofouling in

94   NF/RO systems by a combination of charged hydrogel-coated PP feed spacers and two-phase

95   flow cleaning.

96

2. Theory of feed spacer coating

98   Biofilms initially grow alongside the feed spacer, and eventually attach to the

99   membrane surface (Baker et al. 1995). The feed spacer is responsible for the accumulation of

100 biomass in the membrane channels. Although numerous studies on membrane surface

101 modification (Vrouwenvelder et al. 2009) exist, the literature on spacer surface modification

102 is less abundant. Surface modifications of feed spacers have been studied using metal

103 coatings, *e.g.* silver and copper (Araújo et al. 2012a, Hausman et al. 2010) or functionalized

104 polymers, *e.g.* polydopamine, polydopamine-g-poly(ethylene glycol) and diglyme plasma

105 coating (Araújo et al. 2012b, Reid et al. 2014).

106   The aforementioned surface coatings showed some limitations. Toxic coatings (silver,

107 copper, biocide etc.) act similarly to chemical cleaning, the first layer of bacterial cells might

108 be killed, but the material from dead bacteria provides nutrients for subsequent bacterial

109 growth (Araújo et al. 2012a). For polydopamine and polydopamine-g-poly(ethylene glycol)

110 coatings, although batch adhesion tests using bacterial solutions or proteins under static

111 conditions showed good anti-biofouling properties, long-term and continuous biofouling

112 experiments demonstrated poor biofouling inhibition (Miller et al. 2012). The results might be

113 related to instability of those polymers during long-term experiments. The potential of more

114 stable hydrophilic coatings to facilitate membrane cleaning is therefore still promising (Miller

115 et al. 2012).   Moreover, polydopamine is amphoteric and differently charged in acidic and

116 basic environments (Liu et al. 2014), and the results suggest that surface charge affects the

117 early attachment of biofouling on the feed spacer surface, since electrostatic interactions

118 between surfaces and the charged outer layer of cell membranes of fouling organisms can play

119 a role. Hydrogel-based materials have been reported to have good anti-biofouling properties

120 and have great potential to be applied as antifouling coatings (Chang et al. 2010). Their

121 antifouling properties might be correlated with the charge, entropic elasticity and strong

122 surface hydration of the hydrogels (Murosaki et al. 2011). Poly ethylene glycol (PEG) based

123 coating materials are well known for their remarkable antifouling properties (Ekblad et al.

124 2008). Cationic polyDMAEMA has also been reported as a potential antimicrobial material

125 (Liu et al. 2007), as has the anionic counterpart polySPMA (Wan et al. 2012).

126   Considering that the net charge of the cell wall of most bacteria that cause biofouling

127 is negative (Bereschenko et al. 2010), it is important to investigate the effect of spacer charge

128 (i.e. coating charge for coated spacers) on biofouling control. In addition, some biofouling

129 organisms secrete bioadhesives, which also consist of charged polysaccharides and proteins

130 (Stanley et al. 1999).

131

132 **3. Experimental section**

133 **3.1. Materials**

134   A polypropylene (PP) feed spacer with a thickness of 0.7 mm was provided by Delstar

135 Technology Inc., UK. 2-hydroxyethyl methacrylate (HEMA), polyethylene glycol

136 methacrylate (PEG$_{10}$MA), 3-sulfopropyl methacrylate potassium salt (SPMA), 2-

137 dimethylaminoethyl methacrylate (DMAEMA), and nutrient broth bacterial culture media

138 were purchased from Sigma-Aldrich Sweden AB. Crystal violet, a Gram-color modified kit

139 for Gram staining was purchased from Merck, Sweden. All chemicals were used without

140 further purification. Bacterial attachment assays were carried out using 12-well polystyrene

141 culture plates sterilized by gamma irradiation (VWR, Sweden). Thin film composite ESNA1-

142 LF2 NF membranes and permeate spacers were obtained from Hydranautics, Oceanside,

143 Californa, USA. Sodium acetate (CH$_3$COONa), sodium nitrate (NaNO$_3$), anhydrous

144 monobasic sodium phosphate (NaH$_2$PO$_4$) and sodium hydroxide (NaOH) were purchased

145 from Sigma-Aldrich (Germany) and used as received.

146

147 **3.2. Plasma-mediated UV-polymerization**

6

148   The grafting of charged hydrophilic polymers onto a PP feed spacer surface using

149   plasma treatment of PP and UV-photopolymerization can be generally divided into two steps

150   (Figure 1). The first step is the activation of the PP surface by oxygen plasma. After 15

151   minutes exposure to oxygen plasma at room temperature, hydroxyl, peroxide and carbonyl

152   functional groups are produced. The second step is the grafting of the monomers onto the

153   activated PP surfaces by UV-polymerization (λ=365 nm).

154   Figure 2 illustrates the preparation of the modified feed spacer by coating with the hydrophilic

155   polymers. Polypropylene feed spacer samples were sonicated for 15 min in acetone to remove

156   residual chemicals from the manufacturing, dried and weighed. The samples were then treated

157   with oxygen plasma (standard plasma-system Pico, Diener, Germany) for 15 min, under

158   approximately 10Pa oxygen partial pressure at approximately 200W. Samples were then

159   immediately incubated in 0.4 M solution of monomers (HEMA and $PEG_{10}MA$, SPMA, or

160   DMAEMA) in water for 24 hours at room temperature. For photopolymerization, the

161   incubated samples were placed immediately without further drying between two transparent

162   quartz discs and irradiated by UV light (λ=365 nm) for 2 hours. The reaction chamber was

163   purged with moist nitrogen gas for 1 min before and during UV-polymerization to prevent

164   interference of oxygen and to prevent the solvent from evaporating. After irradiation, the

165   spacer was soaked in water for 24 hours to remove un-reacted monomers and other chemical

166   residues. The samples were then dried in an incubator at 100 $^{\mathrm{o}}$C for 48 h and weighed. The

167   percentage of grafting (PG) of polymer on the spacers was calculated using the following

168   equation:

169    $$PG(\%) = \frac{w_p - w_0}{w_0} x100\%$$ (1)

170   where w_0 and w_p are the weights of the spacer before and after polymerization, respectively.

171   Three replicates of each test sample were used in this work.

7

172

3.3. Polymer characterization

174   All pristine and hydrogel-coated polypropylene (PP) spacers were characterized using Fourier-Transform Infrared Attenuated Total Reflection (FTIR-ATR) spectroscopy using a Pike MIRacle ATR accessory with a diamond prism in a Vertex70 FT-IR Spectrometer (Bruker, Germany) equipped with a DTGS detector. The samples were pressed against the prism with a swivel tip, which is used for non-plated surfaces and makes it possible to hold the substrate by adjusting or twisting its position on the substrate surface. OPUS 7.2 software was used for data acquisition and processing. The spectra were recorded over the wavenumber range 4600-600 cm^{-1} and at a spectral resolution of 4 cm^{-1}. IR spectra of pristine and hydrogel-coated PP were recorded after polymerization, chemical stability test and post-filtration evaluation, respectively.

184   Surface roughness and topography of pristine and hydrogel-coated PP were examined by a NanoScope IVa Dimension 3100 SPM Atomic Force Microscope (AFM) (Veeco Instruments, Inc., USA). The images were recorded over an area of 5x5 μm^2 in tapping mode in air at a line scan acquisition rate of 1 Hz.

188   In order to measure the wettability of the coatings, SPMA, HEMA-PEG$_{10}$MA, and DMAEMA were polymerized onto intiator-immobilized gold surfaces via surface mediated atom transfer radical polymerization (SI-ATRP). The thickness of these coatings was adjusted to 100 Å. The captive bubble technique was used to measure the contact angle of the hydrated polymer coatings using a Dataphysics OCA35 contact angle analyzer with software SCA22. After equilibrating the coating samples in water for 1 h, the samples were placed facing downwards in a glass container filled with deionized water. 2 µl of air was released to the polymer surfaces by a U-shaped needle under control of a computer system. Three contact angles of the bubble were measured and the values were averaged.

197

3.4. Polymer stability test

199   To evaluate the stability of the grafted polymers in water, acidic and basic

200 environments, and after short- and long-term immersion, hydrogel-coated spacers were

201 incubated in water (pH 5, 7 and 9) for one day, one week and one month. The pH was

202 adjusted by adding hydrochloric acid (0.1 M) and sodium hydroxide (0.1 M) to deionized

203 water (Milli-Q). The temperature used in this study was 5°C to avoid the growth of

204 microorganisms, to exclude any effect of biofouling on the stability of the coating, as the

205 presence of microorganisms might change the pH of system as these secrete metabolites. The

206 weight and IR spectra of the samples were measured before and after incubation. The samples

207 were washed several times in Milli-Q water and dried prior to the measurements. The loss of

208 polymer coating in terms of weight loss (WL) was calculated using:

209 $WL = W_f - W_i$ (2)

210 where W_f and W_i are the weight of the spacer after and before incubation, respectively.

211

3.5. Bacterial attachment assay

213   *Escherichia coli* (CCUG 3274) were cultured in nutrient broth (NB) medium at 37° C

214 by shaking at 170 rpm for 16 hours. Fresh sterile NB medium was then added to the bacterial

215 suspension and the optical density was adjusted to 0.1 (approximately 10^8 cfu/ml) at 600 nm.

216 Four replicates of each feed spacer sample (pristine and hydrogel-coated PPs) were placed in

217 12-well polystyrene plates and 4 ml of bacterial suspension was dispensed to each well. The

218 plates were incubated at 37° C and 75 rpm for 1, 4 or 24 hours. After incubation, the samples

219 were washed several times in Milli-Q water and transferred to a new well plate. 4 ml of

220 crystal violet 0.3% was added to each well. After 15 min incubation at room temperature,

221 samples were gently washed three times by Milli-Q water to remove non-bound bacterial cells

9

222   and extra stain. The washed samples were immersed in a new well plate containing 4 ml of

223   ethanol 95% (v/v) for 20 min to release crystal violet from the bacteria cell walls. The optical

224   density (OD) of the solution in each well was measured at 540 nm.

225   Four replicates of each sample, incubated with fresh sterile NB without bacteria, but

226   otherwise treated similarly, were used as negative controls in this experiment. The optical

227   density of crystal violet from bacteria was corrected by subtracting its mean OD from the

228   negative control prior to statistical analysis. To obtain the images of bacteria on the spacer

229   surfaces, the samples were fixed in 10 mL of 2.5% (v/v) glutaraldehyde for 20 min at room

230   temperature. After washing in Milli-Q water and air-drying, the samples were attached to the

231   sample holder using double-sided carbon tape. The surface of the samples was sprayed by

232   compressed gas to remove any lose particles and debris. Bacteria on the feed spacers were

233   detected by a Phenom (FEI, Eindhoven, Netherlands) desktop scanning electron microscope

234   (SEM). The SEM images are displayed as inverted images to enhance the visibility of the

235   bacteria cells.

236   The relative attachment of bacteria to the hydrogel-coated samples is presented as the

237   optical density of the bacteria at 540 nm (OD_{540nm}) on the spacer surface and normalized to

238   the uncoated spacer. Error bars represent the standard deviation from 4 replicates of each

239   sample. Statistical analysis of these data was carried out using Minitab 16 statistical software.

240   One-way Analysis of Variance (ANOVA) with $\alpha = 5\%$ and Tukey's HSD Post-hoc test were

241   performed to determine the difference between hydrogel-coated and uncoated samples. Values

242   were considered significantly different from each other when *p-value* (p) < 0.05.

243

244   **3.6.   Filtration tests**

245   Figure 3 shows the schematic diagram of the filtration test set-up used. The lower part

246   shows the feed water before entering the filtration cells. Tap water (Enschede, The

10

247   Netherlands) used as feed. Before storage in a 60 liter feed tank, the feed water was filtered by

248   a cartridge filter (1-3 µm polypropylene wound FA10", Purtrex PX01-10, USA). The feed

249   tank was equipped with a floating switch valve to regulate the water level. Storage of the feed

250   water in the feed tank, resulted in a water temperature approximately equal to the room

251   temperature. To promote accelerated biofouling growth, nutrients were added to the feed after

252   the feed tank by using a peristaltic pump (Masterflex L/S pumps, Cole-Palmer Instrument

253   Company, USA). The feed water was then pumped and equally distributed into three lines

254   using a high pressure feed pump (Micropump GAF series, Micropump Inc., Canada).

255   In the upper part of the filtration set-up, a mass flow controller (Cori-Flow,

256   Bronkhorst, The Netherlands: 10 ± 0.02 L/h max), regulated the flow rate within each line and

257   allowed equal feed flow to each vertically positioned filtration cell. The filtration cells were

258   covered from direct light to prevent growth of phototrophic organisms like algae. The feed

259   channel pressure drop of the filtration cell was measured using a differential pressure sensor

260   (EL-Press, Bronkhorst, The Netherlands: ΔP max$=100\pm0.5$ kPa) and the flux was measured

261   using a balance (Mettler-Toledo P3002). The retentate and permeate lines were drained

262   without recirculating the water. During two-phase flow cleaning, nitrogen gas was introduced

263   in the liquid line before the filtration cells, controlled by a mass flow controller (EL-Flow,

264   Bronkhorst, The Netherlands: 500 ± 0.25 mL$_n$/min). The filtration cells were custom-made and

265   manufactured from PMMA plates with a stainless steel frame to allow for operation at

266   moderate pressures (maximum operating pressure of 600 kPag).

267   The filtration test procedures were similar as described in our previous work

268   (Wibisono et al. 2015). Each sample of modified feed spacer was tested in two stages: (1) *a*

269   *fouling stage*; biofouling growth in the spacer-filled channel causing at least 300% FCP

270   increase over the feed channel; and (2) *a cleaning stage*; two-phase flow cleaning to remove

271   biofouling.

272   During the fouling stage, fresh NF membranes were used in each experiment and each

273   hydrogel-coated feed spacer was tested in a separate experimental run. Prior to use, the

274   membranes were soaked in Milli-Q water overnight to remove preservation liquid after which

275   the filtration cells were closed. The liquid superficial velocity was set at 0.11 m/s by mass

276   flow controllers and pump speed, and the TMP was set at 600 kPag. To enhance biofouling

277   growth, nutrients (sodium acetate (CH_3COONa), sodium nitrate ($NaNO_3$), and anhydrous

278   monobasic sodium phosphate (NaH_2PO_4)), were added to the feed water in a molar ratio

279   C:N:P = 100:20:10. The nutrient concentration was set at 1 mg Ac-C/L, aiming at an

280   experimental run of approximately 6-7 days for uncoated feed spacers.

281   The FCP and flux were recorded at least once per day for each filtration cell, and the

282   biofouling growth in the filtration cells was observed daily in situ using optical coherence

283   tomography (OCT) (Ganymede Spectral Domain OCT, Thorlabs GmbH, Germany). The OCT

284   was set at a field of view (B-scans) of x=10 mm and z=1.5 mm, with pixel size 5429x546. As

285   shown in Figure 4, the observation area is located in the middle of the filtration cell (blue

286   square) and the red arrow indicates the scanning direction, which is identical to the flow

287   direction. The refractive index of water (1.33) was used since the light beam passes the wetted

288   biofouling layer in the feed channel. The acquisition time was 2.018 s. All tomograms are

289   presented as obtained, the orange scale intensity is proportional to the intensity of the detected

290   reflection of the raw signal.

291   When the FCP of a specific filtration cell increased by at least 300%, the fouling stage

292   was considered to be complete and the cleaning stage was started. During the cleaning stage,

293   the liquid velocity was set at 0.44 m/s, and nitrogen gas was introduced into the liquid using a

294   mass flow controller at a gas/liquid ratio θ=0.5. The TMP was set at 0 kPag during the 10

295   minutes of two-phase flow cleaning. FCP and flux before and after two-phase flow cleaning

296   were measured, and the cleaning efficiency was calculated based on the recovery of the FCP

12

297 to the initial pressure drop at day 0, and the flux recovery to the clean water flux of the

298 membrane (Wibisono et al. 2015).

299   The two-phase flow cleaning efficiency was represented as FCP-based cleaning

300 efficiency or FCP recovery, which was calculated using:

301 $$\eta_{(FCP)} = \frac{\Delta P_{300\% \, fouled} - \Delta P_{cleaned}}{\Delta P_{300\% \, fouled} - \Delta P_0} \cdot 100\% \qquad (3)$$

302 where ΔP_0 is the initial pressure drop at day 0, $\Delta P_{300\% fouled}$ is the final pressure drop

303 determined just before two-phase flow cleaning and $\Delta P_{cleaned}$ is the pressure drop after two-

304 phase flow cleaning. All ΔP values are normalized to the lowest ΔP_0 of all runs.

305   The flux-based cleaning efficiency is presented as MTC recovery and calculated using:

306 $$\eta_{MTC} = \frac{MTC_{fouled} - MTC_{cleaned}}{MTC_{fouled} - MTC_0} \cdot 100\% \qquad (4)$$

307 where MTC_0 is the initial MTC $= 4.9 \times 10^{-11}$ m/s.Pa (Wibisono et al. 2015), MTC_{fouled} is the

308 final MTC before two-phase flow cleaning, and $MTC_{cleaned}$ is the MTC after two-phase flow

309 cleaning.

310   After the filtration test and subsequent two-phase flow cleaning, the feed spacers were

311 removed from the flow cell and dried in an incubator at 100°C for 24 h. The ATR-FTIR

312 spectra of both pristine and polymer-coated PP were then recorded.

313

314 **4. Results and Discussion**

315 **4.1. Coating characterization**

316   The percentage grafting (PG) of polymer on the feed spacer was calculated using Eq.

317 (1). A slight but consistent ~ 0.32% increase in spacer weight was observed for all hydrogels

318 (Table 1). The change relative to the original spacer weight is small and will not affect the

319 geometry of the feed spacer and its hydrodynamics in the feed channel.

13

320   The FTIR-ATR spectra of pristine PP, oxygen plasma-treated PP and the three hydrogel-

321   coated PPs are shown in Figure 5.

322   As shown in Figure 5, the spectrum of pristine PP is dominated by C-H-stretching

323   modes from CH_2 and CH_3 (3000-2800 cm^{-1}), CH_2 and CH_3 deformations (1456 cm^{-1} and 1374

324   cm^{-1}), skeletal vibrations (1162, 981 and 971 cm^{-1}), and CH_2 rocking (845 and 806 cm^{-1}).

325   After 15 minutes of exposure to oxygen plasma, ester carbonyl (C=O) absorptions from

326   aldehyde, keton and acid groups (1730 cm^{-1}) and carbonyl from amides (1643 cm^{-1}) are

327   observed (Lee et al. 1997). Weak O-H stretching bands from hydroxide (3000-3200 cm^{-1})

328   peroxide (3525 cm^{-1}) are observed as well (Lee et al. 1997). Weak C-O stretching bands from

329   hydroxide and peroxide are visible at 1055 and 1125 cm^{-1}. The presence of polyHEMA-co-

330    $PEG_{10}MA$, polyDMAEMA and polySPMA is confirmed by their C=O ester carbonyl

331   stretching peaks visible at 1712-1726 cm^{-1} in the FTIR spectra, which is absent in the

332   spectrum of the pristine spacer and slowly increases in the plasma-treated PP spectrum.

333   Sulfonate functional group (S=O) from SPMA are observed in the polySPMA spectrum at

334   1041 cm^{-1}. Tertiary amine C-H stretching in polyDMAEMA is observed at 2779 cm^{-1}.

335   Furthermore, skeletal C–O–C vibrations of PEG, SPMA and DMAEMA are found at 1100-

336   1160 cm^{-1}. These results indicate that polyHEMA-co-$PEG_{10}MA$, polyDMAEMA and

337   polySPMA are successfully grafted on the PP spacer surface.

338   The surface roughness and topography of pristine and hydrogel-coated PP spacers

339   were observed by tapping-mode AFM in air (Figure 6).

340   As shown in Figure 6, all hydrogel-coated PP samples exhibit a relatively smooth and

341   homogenous surface compared to pristine PP. The root mean square (RMS) roughnesses of

342   pristine PP, polyHEMA-co-$PEG_{10}MA$-coated PP, polyDMAEMA-coated PP, polySPMA-

343   coated PP are 21.5, 8.1, 10.9 and 15.3 nm, respectively. A more rough topography is observed

344   for both the pristine PP and the oxygen plasma treated PP (not shown), compared to the

14

345   coated feed spacers. Although there is a variation in RMS values of polyHEMA-co-

346   PEG$_{10}$MA, polyDMAEMA, and polySPMA coated spacers, differences are minor and

347   obviously all AFM measurements reproducibly showed that the hydrogel-coated PP feed

348   spacers had smoother surface than the pristine PP.

349

350

351   **4.2. Coating stability**

352   The stability of the polymer coatings was evaluated by measuring their weight and IR

353   spectra after incubation in water at 5 ºC for 1 (data not shown), 7 and 30 days at three

354   different pH values (5, 7 and 9). The weight losses were calculated using Eq. (2) and

355   summarized in Table 2, and the IR spectra are shown in Figure 7.

356   At shorter incubation times (1 and 7 days), the coating showed good chemical stability

357   as indicated by the only small changes (relative to untreated sample) in polymer weight (Table

358   2) and the IR spectra (Figure 7). However, at longer incubation times (30 days), a change in

359   weight and IR spectra of the coatings was clearly visible. The weight changes of the coatings

360   were found higher in acidic and basic environment than in neutral environment (pH 7). This is

361   also visible in the stronger decrease in IR intensities for the coatings exposed for 30 days,

362   compared to those of 7 days exposure. PolyHEMA-co-PEG$_{10}$MA suffered from significant

363   degradation in acidic and basic environments, which is indicated by the higher weight loss

364   and reduced C=O ester carbonyl intensity at 1717 cm^{-1}. In addition, oxidative degradation of

365   the PEG chains (Glastrup 1996) after long exposure to water and acidic and basis environment

366   can occur, as seen as a reduction in the skeletal vibrations of PEG at 1100-1160 cm^{-1}.

367   Although the weight changes of polySPMA and polyDMAEMA in acidic and basic

368   environments were lower than those of polyHEMA-co-PEG$_{10}$MA, the C=O ester carbonyl

369   intensities of polyDMAEMA and polySPMA at 1726 and 1712 cm^{-1} respectively, the

370   sulfonate peak in poly SPMA at 1041 cm^{-1} and the tertiary amine of polyDMAEMA at 2779

371   cm^{-1} were all found to decrease significantly upon exposure to acidic and basic environments

372   as well. The stronger degradation of polymers immersed in acidic and basic environments for

373   longer times might be caused by the increased hydrolytic activity in acidic and basic

374   environments, increasing the loss of hydrophilic polymer chain segments (Li et al. 2008, Loh

375   2013).

376   Understanding the chemical stability of polymers in membrane filtration is important as

377   the polymeric materials might be exposed to different pH conditions during filtration due to

378   water pollution and microbial activity during the filtration process. In relation to the anti-

379   biofouling properties of hydrogel-coated PP spacers investigated in the remainder of this

380   paper, the obtained anti biofouling results are still representative, since the bacterial

381   attachment and filtration tests are conducted up to 7 days, in which the polymer coating shows

382   a stable performance and hardly any degradation.

383

4.3. Bacterial attachment test

385   To quantify the attachment of bacteria on the charged hydrogel coated PP spacers,

386   attachment experiments using *E. coli* were performed. *E. coli* is frequently found in water and

387   an emerging cause of water-borne diseases. It is also a very common model bacteria used in

388   lab experiments due to its rapid growth and inexpensive handling and maintenance. Relative

389   attachment of *E. coli* on both pristine and hydrogel-coated PP spacers after 1, 4 and 24 h of

390   incubation is presented in Figure 8.

391   At shorter incubation time (1 h), relative attachment of *E. coli* was found to be very

392   low on polySPMA-coated PP surfaces, compared to that on pristine PP, but also compared to

393   polyDMAEMA- and polyHEMA-co-PEG$_{10}$MA-coated PP surfaces. The statistical analysis of

394   these bacterial attachment data shows that the attachment on the anionic polySPMA coating

16

395   differs significantly ($p < 0.05$) from that on the neutral polyHEMA-co-PEGMA coating and

396   the pristine PP spacer, but is not significantly different from the cationic polyDMAEMA

397   coating ($p > 0.05$). The bacterial attachment at the surface gradually increased when the

398   incubation time increased. Relative to the uncoated, pristine PP spacer, the PolySPMA and

399   polyHEMA-co-PEG$_{10}$MA-coated spacers show a reduced bacterial attachment of about 50 %

400   ($p > 0.05$) after 24 h of incubation. We hypothesize that this lower attachment can be

401   associated with the higher degree of hydrophilicity of polyHEMA-co-PEG$_{10}$MA and

402   polySPMA. The absence of electrostatic attractive interactions between the *E. coli* cell walls

403   and the hydrogels might also contribute to the lower degree of attachment. In addition, as the

404   net charge of the cell walls of *E. coli* at physiological pH is negative (Li and

405   McLandsborough 1999), a repulsive electrostatic interaction between *E.coli* and the anionic

406   polySPMA can also explain the lower degree of attachment of *E.coli* on the anionic

407   polySPMA. The relatively high bacterial attachment found for the polyDMAEMA-coated PP

408   spacer probably results from attractive electrostatic interactions.

409   SEM imaging revealed the adhesion of *E. coli* colonies on the surface of all feed

410   spacers investigated after 1 h of immersion in bacterial solutions at 37°C (Figure 9).

411   As shown in Figure 9 (top), colonies of *E. coli* attach both to pristine PP and hydrogel-

412   coated PP feed spacers. *E. coli* cells attached abundantly at the surface of pristine PP feed

413   spacers compared to the hydrogel-coated PP feed spacers. Less bacteria cells were observed

414   on the surface of the polyDMAEMA-coated and the polyHEMA-co-PEG$_{10}$MA-coated PP

415   feed spacers, and only very few bacteria cells adhered to the surface of the polySPMA-coated

416   PP feed spacer. The images support the aforementioned conclusion that especially the anionic

417   polySPMA coating minimizes bacteria (*E. coli*) attachment.

418   Another reason that can contribute to the lower degree of attachment of bacteria on the

419   polySPMA-coated spacer, is the more hydrophilic nature of this coating. Contact angles

17

420 cannot be measure accurately on the feed spaces meshes, but captive bubble contact angles of

421 polySPMA, polyHEMA-co-PEG$_{10}$MA and polyDMAEMA prepared via surface mediated

422 atom transfer radical polymerization (SI-ATRP) on intiator-immobilized gold surfaces at 100

423 Å thicknesses were 148±1.2, 138±1.8, and 134±1.8 degrees, respectively (as measured inside

424 the bubble). This indicates that the polySPMA layer is more hydrophilic than the two other

425 (polyDMAEMA and polyHEMA-co-PEG$_{10}$MA). Hydrophilicity is an important parameter in

426 determining the anti-biofouling properties of surfaces; in general, more hydrophilic surfaces

427 have better anti-biofouling properties, due to stronger surface hydration. In polySPMA this

428 results from strong ion-dipole interactions between sulfonate ions and water. Water molecules

429 are attracted electrostatically and reoriented to form a hydration shell, whose displacement is

430 associated with a high enthalpic penalty. The hydration of sulfonates in aqueous solution has

431 been simulated(Vchirawongkwin et al. 2012), with the result that around 5 water molecules

432 were coordinated to each sulfonate ion. Unlike cationic polyDMAEMA, where the hydration

433 is influenced by the pH and greatly reduced at neutral and basic pHdue to deprotonation of the

434 ammonium, the hydration shell of anionic polySPMA is relatively stable at neutral pH, since

435 sulfonic acids are strong (with pKa < 0), and thus their hydration is rather pH insensitive. The

436 high repulsion towards *E.coli* by polySPMA is further enhanced by electrostatic repulsive

437 interactions between the identical negative charges of polySPMA and the bacteria cell wall

438 surfaces which also have a net negative charge. It might be expected that the negatively

439 charged sulfonates interact strongly or form complexes with cations, which could potentially

440 reduce antifouling performance, as is the case for carboxylic acids. However, the difference in

441 structure between carboxylic acids and sulfonates is of considerable importance in this

442 respect: the resonance-stabilized sulfonate has the negative charge delocalized over a larger

443 volume than in the carboxylate. This significantly reduces the tendency of sulfonates to form

444 complexes with cations. For example, calcium and magnesium ions form insoluble

445 precipitates with carboxylates, but not with sulfonates.

446 In this work, the contact angle of pristine PP was not measured due to the small surface area

447 and the non-flat surface. However, it has been reported (Kang et al. 2001) that unmodified PP

448 membranes have a contact angle (sessile drop contact angle measured in air) of 108° which is

449 hydrophobic. This hydrophobic surface might result in increased attachment of *E. coli* via

450 hydrophobic interactions.

451

452

4.4. Filtration test and two-phase flow cleaning

4.4.1. Dynamics of feed channel pressure drop and water flux

455 Feed channel pressure drop and MTC dynamics during filtration (fouling stage and

456 two-phase flow cleaning) using pristine PP spacers and the coated PP spacers are shown in

457 Figure 10.

458 As shown in the left panel of Figure 10, the growth of biofouling in the feed spacer

459 channels is shown as an increase in feed channel pressure drop (FCP). An exponential growth

460 is observed for uncoated PP, polyHEMA-co-PEG$_{10}$MA-, and polyDMAEMA- coated feed

461 spacers. The FCP increase of the polyDMAEMA-coated feed spacer shows a significant

462 increase between Day 2 and Day 4 especially. As the fouling stage is considered to be

463 completed when the FCP increase is at least 300%, on Day 4, two-phase flow cleaning was

464 carried out for this polyDMAEMA-coated feed spacer. Longer operation times are required to

465 achieve similar FCP increase for pristine PP and polyHEMA-co-PEG$_{10}$MA-coated PP feed

466 spacers. Interestingly, a long-lasting and linear increase in pressure drop was observed for the

467 polySPMA-coated feed spacer. In contrast to the results observed for the other spacers, the

468 FCP increase for the polySPMA-coated feed spacer develops very slowly and only after one

19

469   week of operation (Day 7), an FCP increase of 300% is reached (an increase from an initial

470   FCP of 19 mbar to 60 mbar).

471   On the other hand, as shown in the right panel of Figure 10, the MTC decrease shows

472   a similar behavior for both uncoated and polymer-coated PP spacers. Consequently, two-

473   phase flow cleaning is able to remove biofouling from the feed spacer channels. However, the

474   MTC recovery due to two-phase flow cleaning is not as high as the FCP recovery (as will be

475   discussed later; see also Figure 12).

476

477   **4.4.2. Daily OCT observations**

478   The biofouling growth during the fouling stage of both uncoated and hydrogel-coated

479   PP spacers is observed daily using optical coherence tomography (OCT). Representative

480   tomograms are shown in Figure 11.

481   As shown in Figure 11, for pristine PP and polyHEMA-co-PEG$_{10}$MA-coated PP feed

482   spacers 6 days are necessary to achieve a 300% FCP increase. The tomograms clearly show

483   the presence of biofouling from day 4 on in these cases, at the region between feed spacer

484   filaments and membrane surface. This region has the lowest flow velocity, and layers of

485   biofilms can develop on top of each other. From day 5 on, biofouling clearly becomes more

486   severe on pristine PP and as well as on polyHEMA-co-PEG$_{10}$MA-coated PP feed spacers.

487   After two-phase flow cleaning on Day 6, the filaments of the polyHEMA-co-PEG$_{10}$MA-

488   coated feed spacer look cleaner than those of the pristine PP feed spacer filaments after two-

489   phase flow cleaning on day 7. This implies that biofouling attached to the polyHEMA-co-

490   PEG$_{10}$MA-coated PP feed spacer surface is easier to remove by two-phase flow cleaning than

491   that on the pristine PP feed spacer.

492   For the polyDMAEMA-coated PP feed spacer, a steep increase in FCP was observed

493   between Day 2 and Day 4. The OCT images support this and a large biofouling matrix is

20

494 clearly observed, mainly in the regions around the feed spacer filaments. Two-phase flow

495 cleaning removed the majority of the biofouling, but still a lot remained. As the net charge of

496 bacteria commonly causing biofouling is negative (Bereschenko et al. 2010), strong adhesion

497 to the positively charged polyDMAEMA-coated spacers occurs. Oppositely, the strong

498 repulsion between bacteria and the negatively charged polySPMA-coated PP feed spacer

499 account for the much better anti fouling properties of this hydrogel coated spacer. During the

500 7 days fouling stage, significant biofouling development on the surface of polySPMA-coated

501 feed spacer filaments is not observed. The effect of two-phase flow cleaning is obvious, when

502 we compare the OCT tomogram of the cleaned polySPMA channel with the pristine channel

503 at day 0. The hydrophilic polySPMA-coated PP feed spacer is very well suited for easy

504 biofouling removal using two-phase flow.

505

506 **4.4.3. Efficiency of two-phase flow cleaning**

507 The efficiency of the applied two-phase flow cleaning in terms of FCP and MTC

508 recovery is calculated based on both FCP and MTC data using Eq. (3) and Eq. (4) and

509 presented in Figure 12.

510 In terms of FCP recovery, two-phase flow cleaning is rather effective and powerful to

511 remove a large part of the biofouling from the spacer-filled channel itself, regardless of the

512 presence or absence of a feed spacer coating. The FCP level after two-phase flow cleaning is

513 between 0.5-0.9 kPag, although the FCP value before the two-phase flow cleaning was very

514 high (see Figure 10 left panel). When comparing the FCP data of all different spacers, the

515 FCP recovery is equal for all spacer types and recoveries of 60 to 70% are obtained.

516 Regarding MTC recovery, pristine PP and polySPMA-coated PP feed spacers yield

517 flux recoveries of about 60%, while polyDMAEMA- and polyHEMA-co-PEG$_{10}$MA-coated

518 PP feed spacers generate lower flux recoveries, below 40%. Initially, all systems had the same

21

519   initial flux (as all use the same membrane). However, to reach an FCP increase of 300%,

520   different operation times are required depending on the type of spacer. For polySPMA-coated

521   PP feed spacers, a 300% FCP increase was reached after 7 days and during that period, the

522   flux in terms of MTC value decreased to $0.86 \cdot 10^{-11}$ m/s·Pa. After two-phase flow cleaning, the

523   MTC recovered to approximately $3.11 \cdot 10^{-11}$ m/s·Pa, which is close to the initial MTC_0 value

524   of $4.9 \cdot 10^{-11}$ m/s·Pa. The OCT image of the polySPMA-coated PP feed spacer after cleaning

525   supports this and shows an almost identically clean feed channel as on day 0 (see Figure 11).

526   Similar behavior is observed for pristine PP. For polyHEMA-co-PEG_{10}MA-coated PP feed

527   spacers, although the MTC of the fouled system is identical to the MTC value of the fouled

528   polySPMA-coated PP and pristine PP, the MTC recovery after two-phase flow cleaning is

529   lower. This is the same for polyDMAEMA-coated PP spacers, since also in this case the

530   filtration time to reach 300% FCP increase is relatively short, resulting in relatively high MTC

531   values when two-phase flow cleaning was applied, resulting in low MTC recoveries.

532   Based on the FCP- and MTC-recovery data, especially the anionic polySPMA-coated

533   PP feed spacers showed delayed biofouling growth and a delayed FCP increase, resulting in a

534   reduced need for two-phase flow cleaning.

535

536   **4.5. Post-filtration analysis**

537   Foulant characteristics on the surfaces of pristine and hydrogel-coated PP spacers were

538   evaluated by determining the change in weight due to biofouling attachment and measuring

539   the IR spectra of the samples after being exposed to filtration experiments up to 7 days and

540   subsequent two-phase flow cleaning. The FTIR-ATR spectra were recorded after the samples

541   were air dried at room temperature. Spectra are shown in Figure 13.

542   The N-H band of Amide A is normally seen at 3270-3310 cm^{-1} (Creighton 2002, Khan

543   et al. 2013, Krimm and Bandekar 1986, Krimm and Dwivedi 1982) and its specific IR

22

544 frequencies depend on the structure of the amino acids present. For example, α-Poly-alanine

545 has an N-H stretching bond of the amide A near 3300 cm^{-1} (Rabolt et al. 1977), for

546 polyglycine II this is 3303 cm^{-1} (Dwivedi and Krimm 1982) and for Ca-poly(L-glutamate) this

547 can be found at 3275 cm^{-1} (Sengupta et al. 1984). In this work, prominent signals of the N-H

548 band of Amide A are clearly observed at 3284-3290 cm^{-1} on the surface of pristine PP,

549 polyDMAEMA-coated and polyHEMA-co-PEG$_{10}$MA-coated PP spacers (Fig. 13).

550 Furthermore, on these three samples, amide I and II are also observed at 1641-1653 cm^{-1} and

551 1537-1543 cm^{-1}, respectively. These results suggest the presence of proteins on the surface of

552 pristine PP, polyDMAEMA and polyHEMA-co-PEG$_{10}$MA spacers. The presence of a

553 phosphodiester backbone of nucleic acid is clearly found for pristine PP and polyDMAEMA

554 surfaces, as suggested by the bands at 1236 and 1238 cm^{-1}. In addition, the peak at 1080 cm^{-1}

555 faintly found on pristine PP suggests the presence of C-O and C-O-C from sugars (Khan et al.

556 2013). These results suggest the presence of biological materials on the surface of pristine PP,

557 polyDMAEMA and polyHEMA-co-PEG$_{10}$MA. Interestingly, these fingerprints were not

558 found on the surface of the polySPMA-coated PP spacers and supports the previous results

559 obtained from bacterial attachment experiments, FCP and MTC data and OCT images.

560 The foulants on the surface of pristine and polymer-coated PP spacers were visualized

561 by SEM and the images are shown in Figure 14. Foulants were found to be omnipresent on

562 the surface of pristine PP. Fouling was less dominant on the surface of polyHEMA-co-

563 PEG$_{10}$Ma-coated and polyDMAEMA-coated spacers and lowest on the anionic polySPMA-

564 coated spacer. These images also demonstrate that the coating of hydrogels on spacer surfaces

565 and especially the application of an anionic polySPMA coating enhance the performance of

566 the membrane process and the effectiveness of two-phase flow cleaning.

567

568 **5. Conclusion**

23

569   PolyHEMA-co-PEG$_{10}$MA (0), polyDMAEMA (+) and polySPMA (-) were

570   successfully coated on PP feed spacer surfaces via plasma mediated UV-polymerization.

571   These coatings are chemically stable for at least 7 days upon immersion into neutral, acidic

572   and basic environments. All hydrogel-coated PP samples showed improved anti-biofouling

573   properties during bacterial attachment tests. During filtration experiments, polyDMAEMA

574   shows low anti-biofouling properties due to hydrophobic interactions. The performance of

575   polyHEMA-co-PEG$_{10}$MA is fairly good. PolySPMA-coated PP feed spacers on the contrary

576   show significant anti-biofouling properties. Employing this highly hydrophilic surface during

577   removal of biofouling by two-phase flow cleaning also showed enhanced cleaning efficiency,

578   feed channel pressure drop and flux recoveries. A combination of polySPMA-coated PP feed

579   spacers and two-phase flow cleaning therefore is promising and an environmentally friendly

580   approach to control biofouling in NF/RO systems employing spiral-wound membrane

581   modules. However, would be also interesting to compare the antifouling performance of this

582   anionic PSPMA with the well-known nonfouling zwitterionic or mixed-charged coatings in

583   future work.

584

585

Acknowledgments

24

593   supported by the European Community's Seventh Framework Program FP7/2007–2013 under

594   Grant Agreement number [237997] (SEACOAT).

595

596   **Note**

597   Yusuf Wibisono and Wetra Yandi contributed equally to this work.

598

599   **Nomenclature**

600	FCP	$= \Delta P =$ feed channel pressure drop	[Pa]
601	ΔP_0	= initial feed channel pressure drop	[Pa]
602	ΔP_{fouled}	= feed pressure drop over the fouled channel	[Pa]
603	$\Delta P_{cleaned}$	= feed channel pressure drop after two-phase flow cleaning	[Pa]
604	MTC	= mass transfer coefficient	[m/Pa.s]
605	TMP	= trans-membrane pressure	[Pa]
606	u_L	= superficial liquid velocity	[m/s]
607	η	= two-phase flow cleaning efficiency	[%]
608	θ	= gas/liquid ratio	[-]

609

610

611   **References**

612   Applegate, L.E., Erkenbrecher Jr, C.W. and Winters, H. (1989) New chloroamine process to

613   control aftergrowth and biofouling in permasepR B-10 RO surface seawater plants.

614   Desalination 74(0), 51-67.

615   Araújo, P.A., Kruithof, J.C., Van Loosdrecht, M.C.M. and Vrouwenvelder, J.S. (2012a) The

616   potential of standard and modified feed spacers for biofouling control. Journal of Membrane

617   Science 403-404, 58-70.

25

618 Araújo, P.A., Miller, D.J., Correia, P.B., Van Loosdrecht, M.C.M., Kruithof, J.C., Freeman,

619 B.D., Paul, D.R. and Vrouwenvelder, J.S. (2012b) Impact of feed spacer and membrane

620 modification by hydrophilic, bactericidal and biocidal coating on biofouling control.

621 Desalination 295, 1-10.

622 Baker, J., Stephenson, T., Dard, S. and Côté, P. (1995) Characterisation of Fouling of

623 Nanofiltration Membranes used to Treat Surface Waters. Environmental Technology 16(10),

624 977-985.

625 Bereschenko, L., Stams, A., Euverink, G. and van Loosdrecht, M. (2010) Biofilm formation

626 on reverse osmosis membranes is initiated and dominated by Sphingomonas spp. Applied and

627 environmental microbiology 76(8), 2623-2632.

628 Bereschenko, L.A., Prummel, H., Euverink, G.J.W., Stams, A.J.M. and van Loosdrecht,

629 M.C.M. (2011) Effect of conventional chemical treatment on the microbial population in a

630 biofouling layer of reverse osmosis systems. Water Research 45(2), 405-416.

631 Chang, Y., Yandi, W., Chen, W.-Y., Shih, Y.-J., Yang, C.-C., Chang, Y., Ling, Q.-D. and

632 Higuchi, A. (2010) Tunable Bioadhesive Copolymer Hydrogels of Thermoresponsive Poly(N-

633 isopropyl acrylamide) Containing Zwitterionic Polysulfobetaine. Biomacromolecules 11(4),

634 1101-1110.

635 Creber, S.A., Vrouwenvelder, J.S., van Loosdrecht, M.C.M. and Johns, M.L. (2010) Chemical

636 cleaning of biofouling in reverse osmosis membranes evaluated using magnetic resonance

637 imaging. Journal of Membrane Science 362(1–2), 202-210.

638 Creighton, T.E. (2002) Proteins : Structures and molecular properties W.H. Freeman and

639 Company, New York.

640 Dwivedi, A.M. and Krimm, S. (1982) Vibrational Analysis of Peptides, Polypeptides, and

641 Proteins .15. Crystalline Polyglycine-Ii. Biopolymers 21(12), 2377-2397.

642 Ekblad, T., Bergström, G., Ederth, T., Conlan, S.L., Mutton, R., Clare, A.S., Wang, S., Liu,

643 Y., Zhao, Q., D'Souza, F., Donnelly, G.T., Willemsen, P.R., Pettitt, M.E., Callow, M.E.,

644 Callow, J.A. and Liedberg, B. (2008) Poly(ethylene glycol)-Containing Hydrogel Surfaces for

645 Antifouling Applications in Marine and Freshwater Environments. Biomacromolecules 9(10),

646 2775-2783.

647 Glastrup, J. (1996) Degradation of polyethylene glycol. A study of the reaction mechanism in

648 a model molecule: Tetraethylene glycol. Polymer Degradation and Stability 52(3), 217-222.

649 Greenlee, L.F., Lawler, D.F., Freeman, B.D., Marrot, B. and Moulin, P. (2009) Reverse
650 osmosis desalination: Water sources, technology, and today's challenges. Water Research
651 43(9), 2317-2348.

652 Hausman, R., Gullinkala, T. and Escobar, I.C. (2010) Development of copper-charged
653 polypropylene feedspacers for biofouling control. Journal of Membrane Science 358(1-2),
654 114-121.

655 Hijnen, W.A.M., Castillo, C., Brouwer-Hanzens, A.H., Harmsen, D.J.H., Cornelissen, E.R.
656 and van der Kooij, D. (2012) Quantitative assessment of the efficacy of spiral-wound
657 membrane cleaning procedures to remove biofilms. Water Research 46(19), 6369-6381.

658 Hilal, N., Al-Zoubi, H., Darwish, N.A., Mohammad, A.W. and Abu Arabi, M. (2004) A
659 comprehensive review of nanofiltration membranes: Treatment, pretreatment, modelling, and
660 atomic force microscopy. Desalination 170(3), 281-308.

661 Kang, M.S., Chun, B. and Kim, S.S. (2001) Surface modification of polypropylene membrane
662 by low-temperature plasma treatment. Journal of Applied Polymer Science 81(6), 1555-1566.

663 Khan, M.T., Manes, C.L.D., Aubry, C. and Croue, J.P. (2013) Source water quality shaping
664 different fouling scenarios in a full-scale desalination plant at the Red Sea. Water Research
665 47(2), 558-568.

666 Krimm, S. and Bandekar, J. (1986) Vibrational Spectroscopy and Conformation of Peptides,
667 Polypeptides, and Proteins. Advances in Protein Chemistry 38, 181-364.

668 Krimm, S. and Dwivedi, A.M. (1982) Vibrational Analysis of Peptides, Polypeptides and
669 Proteins .12. Fermi Resonance Analysis of the Unperturbed Nd Stretching Fundamental in
670 Polypeptides. Journal of Raman Spectroscopy 12(2), 133-137.

671 Lee, S.D., Sarmadi, M., Denes, F. and Shohet, J.L. (1997) Surface modification of
672 polypropylene under argon and oxygen-RF-plasma conditions. Plasmas and Polymers 2(3),
673 177-198.

674 Li, J., Jiang, G. and Ding, F. (2008) The effect of pH on the polymer degradation and drug
675 release from PLGA-mPEG microparticles. Journal of Applied Polymer Science 109(1), 475-
676 482.

677 Li, J. and McLandsborough, L.A. (1999) The effects of the surface charge and hydrophobicity
678 of Escherichia coli on its adhesion to beef muscle. International Journal of Food Microbiology
679 53(2–3), 185-193.

680   Liu, G.M., Wu, D., Ma, C.C., Zhang, G.Z., Wang, H.F. and Yang, S.H. (2007) Insight into the

681   origin of the thermosensitivity of poly[2-(dimethylamino)ethyl methacrylate]. Chemphyschem

682   8(15), 2254-2259.

683   Liu, Y., Ai, K. and Lu, L. (2014) Polydopamine and Its Derivative Materials: Synthesis and

684   Promising Applications in Energy, Environmental, and Biomedical Fields. Chemical

685   Reviews.

686   Loh, X.J. (2013) The effect of pH on the hydrolytic degradation of poly(ε-caprolactone)-

687   block-poly(ethylene glycol) copolymers. Journal of Applied Polymer Science 127(3), 2046-

688   2056.

689   Matin, A., Khan, Z., Zaidi, S.M.J. and Boyce, M.C. (2011) Biofouling in reverse osmosis

690   membranes for seawater desalination: Phenomena and prevention. Desalination 281(0), 1-16.

691   Miller, D.J., Araújo, P.A., Correia, P.B., Ramsey, M.M., Kruithof, J.C., van Loosdrecht,

692   M.C.M., Freeman, B.D., Paul, D.R., Whiteley, M. and Vrouwenvelder, J.S. (2012) Short-term

693   adhesion and long-term biofouling testing of polydopamine and poly(ethylene glycol) surface

694   modifications of membranes and feed spacers for biofouling control. Water Research 46(12),

695   3737-3753.

696   Murosaki, T., Ahmed, N. and Gong, J.P. (2011) Antifouling properties of hydrogels. Science

697   and Technology of Advanced Materials 12(6).

698   Rabolt, J.F., Moore, W.H. and Krimm, S. (1977) Vibrational Analysis of Peptides,

699   Polypeptides, and Proteins .3. Alpha-Poly(L-Alanine). Macromolecules 10(5), 1065-1074.

700   Reid, K., Dixon, M., Pelekani, C., Jarvis, K., Willis, M. and Yu, Y. (2014) Biofouling control

701   by hydrophilic surface modification of polypropylene feed spacers by plasma polymerisation.

702   Desalination 335(1), 108-118.

703   Sengupta, P.K., Krimm, S. and Hsu, S.L. (1984) Vibrational Analysis of Peptides,

704   Polypeptides, and Proteins .21. Beta-Calcium-Poly(L-Glutamate). Biopolymers 23(8), 1565-

705   1594.

706   Stanley, M.S., Callow, M.E. and Callow, J.A. (1999) Monoclonal antibodies to adhesive cell

707   coat glycoproteins secreted by zoospores of the green alga Enteromorpha. Planta 210(1), 61-

708   71.

709   Vchirawongkwin, V., Pornpiganon, C., Kritayakornupong, C., Tongraar, A. and Rode, B.M.

710   (2012) The Stability of Bisulfite and Sulfonate Ions in Aqueous Solution Characterized by

711   Hydration Structure and Dynamics. Journal of Physical Chemistry B 116(37), 11498-11507.

712   Vrouwenvelder, J.S., Graf von der Schulenburg, D.A., Kruithof, J.C., Johns, M.L. and van

713   Loosdrecht, M.C.M. (2009) Biofouling of spiral-wound nanofiltration and reverse osmosis

714   membranes: A feed spacer problem. Water Research 43(3), 583-594.

715   Wan, F., Pei, X., Yu, B., Ye, Q., Zhou, F. and Xue, Q. (2012) Grafting Polymer Brushes on

716   Biomimetic Structural Surfaces for Anti-Algae Fouling and Foul Release. ACS Applied

717   Materials & Interfaces 4(9), 4557-4565.

718   Wibisono, Y., Cornelissen, E.R., Kemperman, A.J.B., van der Meer, W.G.J. and Nijmeijer, K.

719   (2014) Two-phase flow in membrane processes: A technology with a future. Journal of

720   Membrane Science 453(0), 566-602.

721   Wibisono, Y., El Obied, K.E., Cornelissen, E.R., Kemperman, A.J.B. and Nijmeijer, K.

722   (2015) Biofouling removal in spiral-wound nanofiltration elements using two-phase flow

723   cleaning. Journal of Membrane Science 475(0), 131-146.

724

725

Table 1. Percentage grafting of polymer-coated PP feed spacer.

Polymer type	PG (%)
HEMA-co-PEG$_{10}$MA	0.3203 ± 0.051
DMAEMA	0.3203 ± 0.064
SPMA	0.3205 ± 0.054

Table 2. The stability of the hydrogel polymer coating on the PP spacers evaluated by measuring the weight loss of the polymer coating only on the PP spacer after 7 and 30 days incubation in buffer solution at pH 5, 7 and 9**.** The errors represent the standard deviations from three replicates of each sample.

Coating	Weight loss (mg)					
	7 days incubation			30 days incubation		
	pH 5	pH 7	pH 9	pH 5	pH 7	pH 9
polyHEMA-co-PEG$_{10}$MA	0.13 ± 0.07	0.10 ± 0.00	0.10 ± 0.00	0.30 ± 0.10	0.20 ± 0.00	0.30 ± 0.10
polyDMAEMA	0.10 ± 0.00	0.10 ± 0.00	0.17 ± 0.07	0.23 ± 0.11	0.20 ± 0.00	0.17 ± 0.07
polySPMA	0.10 ± 0.00	0.10 ± 0.00	0.13 ± 0.07	0.17 ± 0.07	0.17 ± 0.06	0.17 ± 0.06
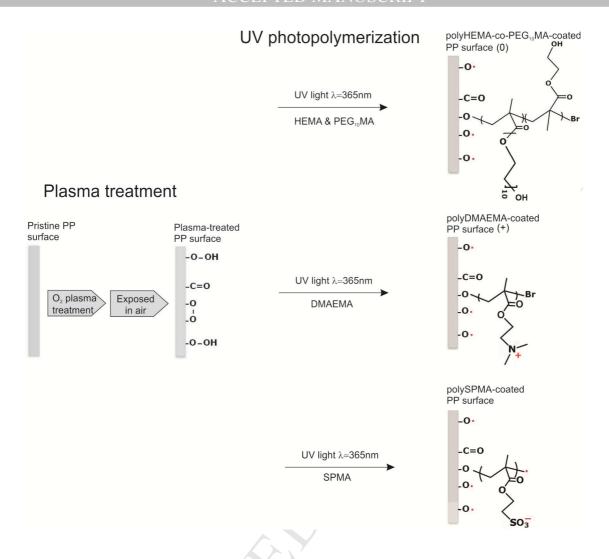
Fig. 1. Reaction scheme of UV-induced grafted polymerization (UV light, λ=365 nm) of hydrophilic polymers (polyHEMA-co-PEG10MA, polyDMAEMA or polySPMA) onto a polypropylene (PP) feed spacer surface. PP is treated in oxygen plasma, followed by UV irradiation to attached the monomers (i.e. HEMA/PEG10MA mixture, DMAEMA, or SPMA). The resulting hydrogel polymers grafted to the PP surface have different charges: polyHEMA-co-PEG10MA is neutral (0), polyDMAEMA has a positive charge (+) and polySPMA has a negative charge (-)
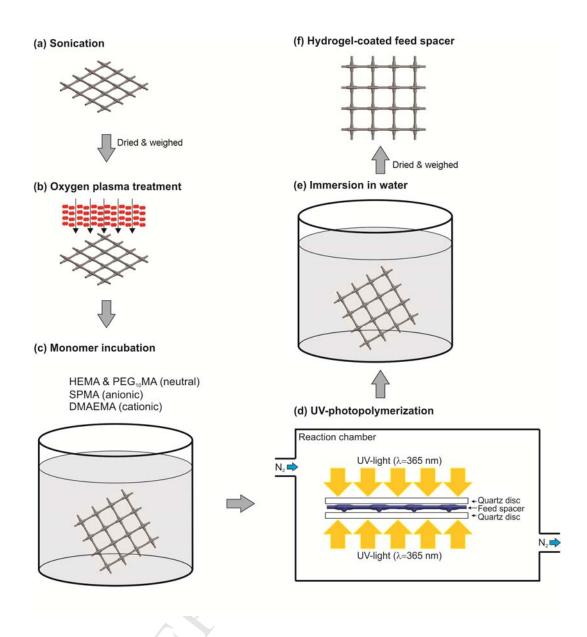
Fig. 2. Plasma mediated UV-polymerization of hydrophilic polymers on polypropylene feed spacers: (a) sonication, 15 min in acetone; (b) oxygen plasma treatment for 15 min; (c) incubation in monomer solution (HEMA and $PEG_{10}MA$, DMAEMA, or SPMA) for 24 hours; (d) UV-polymerization (λ=365nm) for 2 hours; (e) soaking in water for 24 hours; (f) hydrophilized feed spacer after drying.
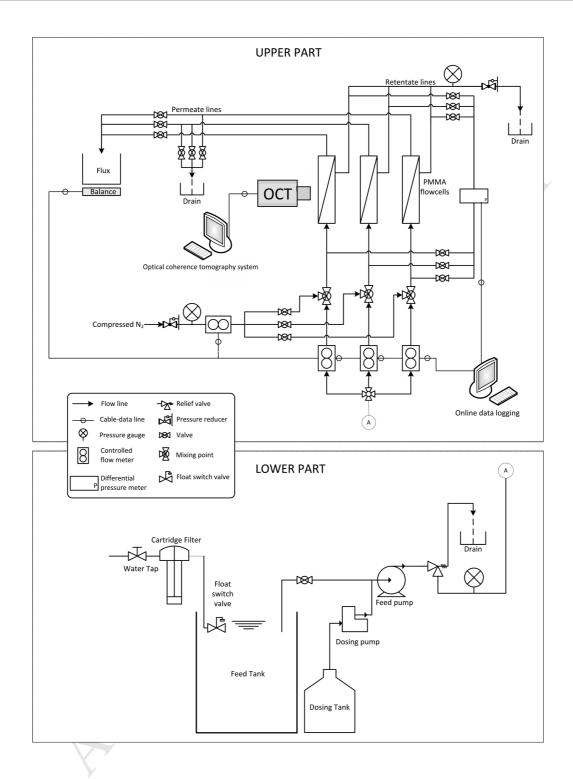
Fig. 3. Experimental set-up used for filtration experiments. The lower part consists of a water tap, cartridge filter, feed tank, dosing tank, dosing pump and feed pump. The upper part consists of mass flow controllers, filtration cells, differential pressure meters, balance and nitrogen gas line; all measurements were controlled and logged using a personal computer. The biofouling growth was observed daily by optical coherence tomography (OCT).
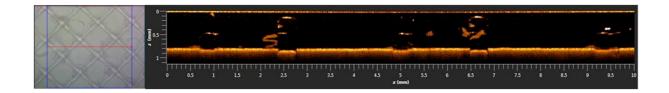
Fig. 4. *Left*: OCT observation of biofouling in the spacer-filled channels in the middle of the filtration cell; the blue square indicates the observation area and the red arrow is the scan direction, which is in the same direction as the flow direction. *Right*: OCT image showing a 2-D cross-sectional view of the biofouling structure in a spacer-filled filtration channel, exactly at the red line shown in the left picture. Refractive index is 1.33 and the intensity of the detected reflection of the raw signal is presented as the orange scale intensity. Field of view (FOV): x=10 mm and z=1.5 mm, with pixel size 5429x546 and acquisition time 2.018 s.
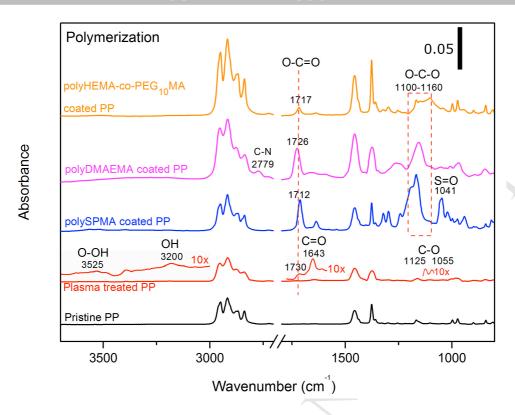
Fig. 5. FTIR-ATR spectra of pristine PP, oxygen plasma-treated PP and hydrogel-coated PP (polyHEMA-co-PEG$_{10}$MA, polyDMAEMA and polySPMA). The floating bar in right upper corner is the absorbance scale unit.
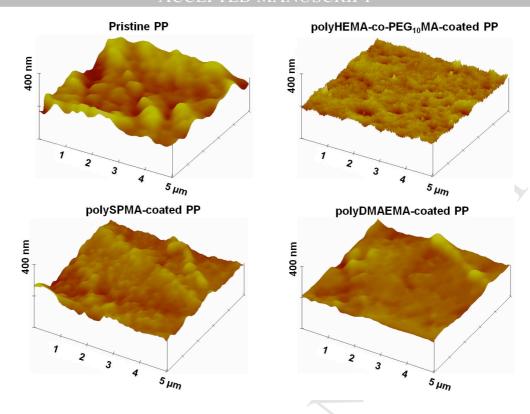
Fig. 6. Surface topography of pristine PP and charged-hydrogel (polyHEMA-co-PEG$_{10}$MA, polyDMAEMA and polySPMA) coated PP feed spacers, measured by tapping mode AFM in air over 5x5 µm^2 areas at an acquisition rate of 1 Hz.
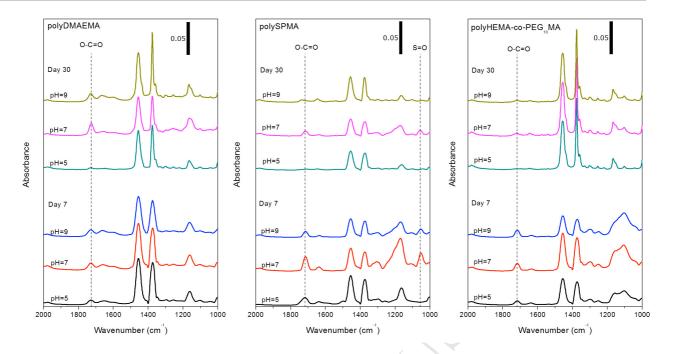
Fig.7. FTIR-ATR spectra of hydrogel-coated (polyHEMA-co-PEG$_{10}$MA, polyDMAEMA and polySPMA) PP spacers after incubation in water for 7 and 30 days at three different pH values (5, 7 and 9). Floating bars in the right upper corner of each spectrum is the absorbance scale unit.
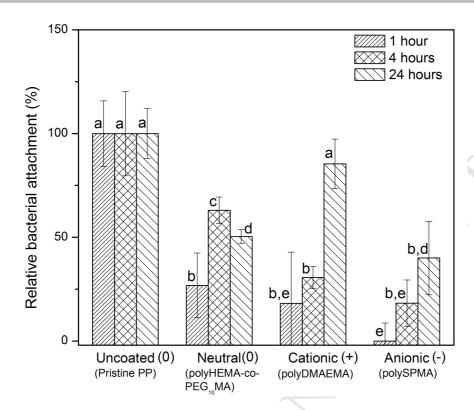
Fig. 8. Relative attachment of *E. coli* cells on pristine and polymer coated PP feed spacer surfaces after 1, 4, and 24 h of immersion in bacterial solutions at 37°C. Error bars indicate the standard deviation obtained from four replicates. The different letters above the bars indicate whether the data are significantly different to each other at $p < 0.05$.

Pristine PP

polyHEMA-co-PEG$_{10}$MA

polyDMAEMA

polySPMA
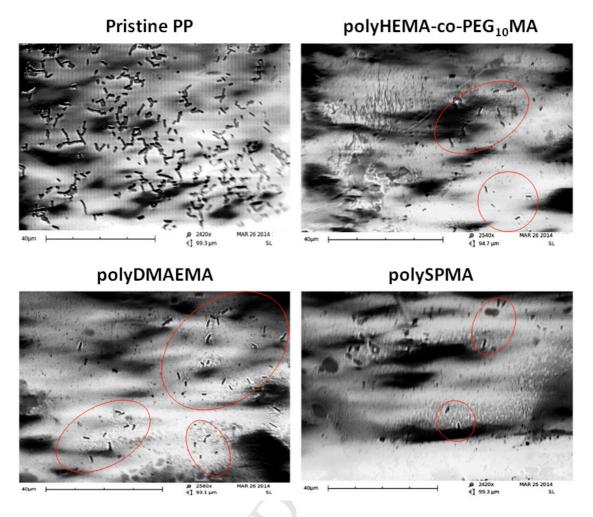
Fig. 9. *E. coli* cells attached on pristine and coated PP feed spacer surfaces after 1 h of immersion in bacterial solutions at 37°C as observed by SEM (scale bar length is 40 μm). Colonies of bacteria cells adhered on polyDMAEMA-, polyHEMA-co-PEG$_{10}$MA- and polySPMA-coated PP feed spacers are shown highlighted in the red circles.
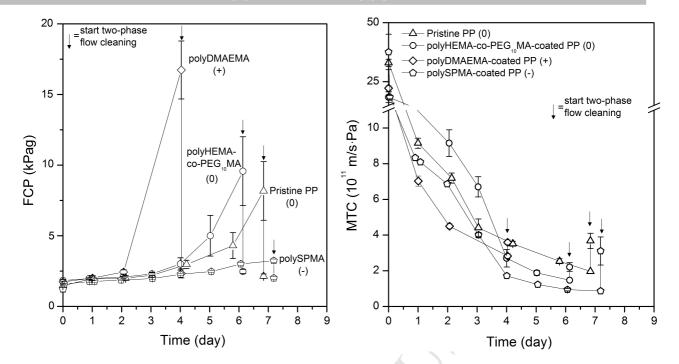
Fig. 10. *Left*: Feed channel pressure drop (FCP) during biofouling in filtration cells with different feed spacer coatings (pristine PP, polyHEMA-co-PEG$_{10}$MA (0), polyDMAEMA (+) and polySPMA (-)), and cleaning by two-phase flow (indicated by arrow). *Right*: MTC dynamics (pristine PP, polyHEMA-co-PEG$_{10}$MA, polyDMAEMA and polySPMA spacers) during fouling stage and two-phase flow cleaning (indicated by arrow).
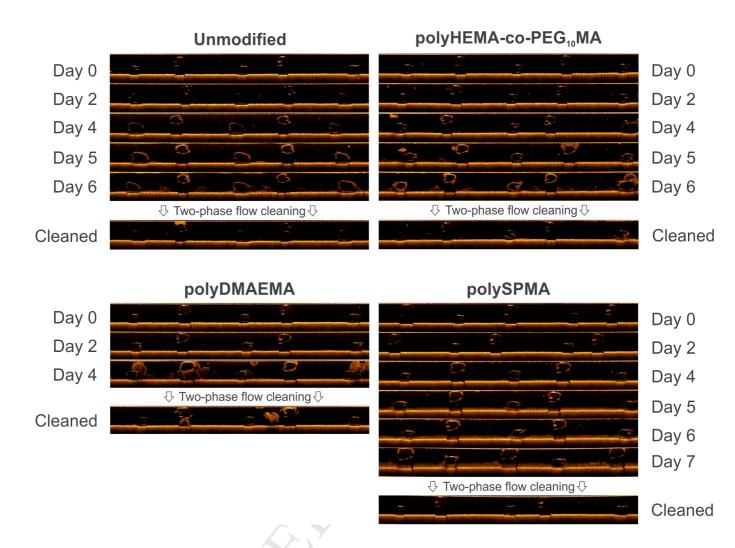
Fig. 11. Series of equidistant OCT images (1.5 mm x 10 mm, resolution 5429x546 pixels, measured daily using the refractive index of water (1.33)) of: pristine, polyHEMA-co-PEG$_{10}$MA-coated, polyDMAEMA-coated, and polySPMA-coated polypropylene feed spacer-filled channels during biofouling and after two-phase flow cleaning. Two-phase flow cleaning was conducted at a liquid velocity of u_L=0.44 m/s and a gas/liquid ratio of θ=0.5. The orange scale intensity is proportional to the intensity of the detected reflection of the raw signal. Pristine PP spacer: two-phase flow cleaning on day 6; polyDMAEMA-coated spacer: two-phase flow cleaning on day 4; polyHEMA-co-PEG$_{10}$MA-coated spacer: two-phase flow cleaning on day 6; polySPMA-coated spacer: two-phase flow cleaning on day 7.
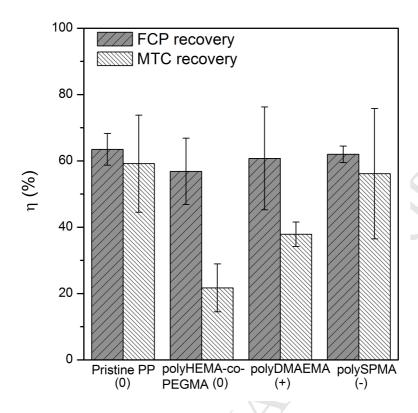
Fig. 12. FCP and MTC recovery by two-phase flow cleaning (pristine PP (0) spacers, polyHEMA-co-PEG$_{10}$MA (0) coated, polyDMAEMA (+) coated and polySPMA (-) coated PP feed spacers).
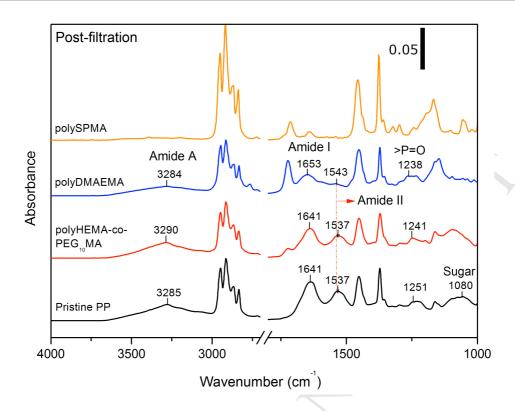
Fig. 13. FTIR-ATR spectra of of pristine PP and the three hydrogel-coated PP spacers after filtration experiments and two-phase flow cleaning. Floating bar in the right upper corner represents the absorbance scale unit.
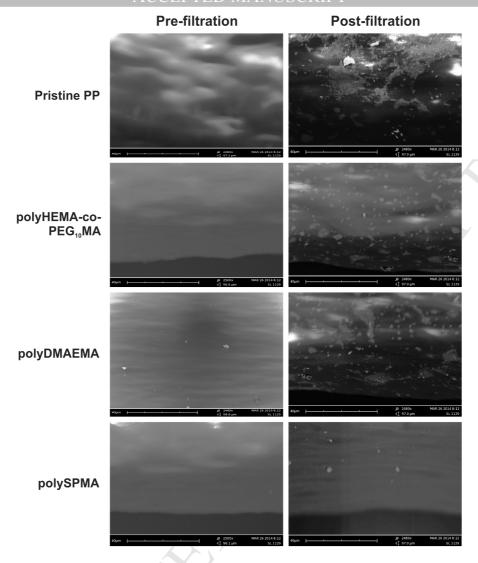
Fig. 14. SEM images of the surface of pristine and polymer-coated PP feed spacers before (*left*) and after (*right*) filtration/two-phase flow cleaning (scale bar length is 40 μm). Abundant amounts of biomass are observed on the pristine PP surface, while less biomass is found on the polymer-coated PP feed spacers, and especially the polySPMA-coated spacer.

Highlights

- A novel platform approach for eco-friendly biofouling mitigation is presented.
- Hydrogel-coated feed spacers and two-phase flow cleaning showed a good biofouling control.
- The surface charge plays important roles on the antibiofouling behavior.
- The coatings are stable after 7 days incubation in neutral, acidic and basic environments.